Analyst

ROYAL SOCIETY OF CHEMISTRY

PAPER

View Article Online
View Journal | View Issue

Check for updates

Cite this: *Analyst*, 2021, **146**, 7265

In situ assessment of mitochondrial respiratory activity and lipid metabolism of mouse oocytes using resonance Raman spectroscopy

Mika Ishigaki, *[a,b] Shinsuke Kashiwagi,[c] Satoru Wakabayashi[c] and Yumi Hoshino*[d]

This study aimed to develop a method to determine the degree of oocyte maturation in metaphase II *in situ* based on the balance between mitochondrial respiratory activity and lipid metabolism using resonance Raman spectroscopy. A decrease in the respiratory activity of overmatured oocytes was indicated by the reduced intensities of the resonance Raman bands corresponding to reduced cytochrome *c* in the cytoplasm. Moreover, the increased lipid concentration in overmature oocytes indicated lower lipid metabolism with a decreased mitochondrial function. New indexes were defined in terms of the ratios of the representative Raman peak intensities of reduced cytochrome *c* (750 and 1127 cm^{-1}) to those of lipids (1438 cm^{-1}) and they successfully classify the oocytes into groups based on their quality, which varied with their maturation degree. The high development rate of embryos that were fertilized *in vitro* after laser irradiation showed that laser irradiation was noninvasive to oocytes. The evaluation of two factors *in situ*, the active respiration and lipid metabolism, means to catch the most fundamental biochemical reactions of life activities. Our results demonstrate the potential application of resonance Raman spectroscopy as a new, noninvasive, and universal cell evaluation technology, for not only oocytes but also more general cells such as somatic cells and iPS cells.

Received 23rd June 2021,
Accepted 8th October 2021

DOI: 10.1039/d1an01106e

rsc.li/analyst

Published on 04 November 2021. Downloaded on 7/17/2025 3:33:19 PM.

Introduction

Oocyte quality is an intrinsically important factor that affects the success rate of infertility treatment in humans. A novel technology to assess oocyte quality is required worldwide. The degree of oocyte maturity is one of the factors that determines oocyte quality. An oocyte suspends its meiosis in metaphase II (MII) after ovulation and waits to be fertilized. Even during the suspension of meiosis, *in ovo* substances change from moment to moment to adapt to fertilization.[1–3] However, the observation of morphological features, such as the shape of the spindle and the polar body, under a microscope is currently the only nondestructive means of determining the optimal fertilization period. Therefore, a novel evaluation technique is required to assess oocyte quality based on *in situ* molecular information.

Raman spectra reflect molecular information, such as the concentration and structure of proteins, lipids, and DNA, and they can be nondestructively obtained *in situ* without labeling even from complicated biological systems. Thus, Raman spectroscopy has been actively studied for its biological and medical applications.[4–6] For example, Chan *et al.* used single-cell micro-Raman spectroscopy to discriminate neoplastic cells from human lymphocytes.[7] The differences in the Raman spectra between DNA and proteins were used to distinguish normal lymphocytes from neoplastic lymphocytes. Tan *et al.* found distinct differences between the Raman spectra of human induced pluripotent stem (iPS) cells and differentiated human embryonic stem (ES) cells resulting from changes in intracellular substances associated with the differentiation of ES cells.[8] Raman measurements using a 532 nm excitation wavelength are particularly suitable for the analysis of cytochromes in living cells. Okada *et al.* reported label-free Raman imaging of HeLa cell apoptosis using 532 nm excitation.[9] Kakita *et al.* used resonance Raman signals obtained from cytochromes to quantify the reduction states of cytochromes *b* and *c* in *Saccharomyces cerevisiae* cells.[10]

Raman spectroscopy has been used to study oocytes or embryos.[11–15] Bogliolo *et al.* studied aging-related oxidative damage in the mouse MII phase, and young oocytes were distinguished from old oocytes by performing a principal component analysis (PCA) of lipid and protein Raman bands.[12] Heraud *et al.* reported the changes of macromolecular architec-

[a]*Institute of Agricultural and Life Sciences, Academic Assembly, Shimane University, 1060 Nishikawatsu, Matsue, Shimane, 690-8504, Japan. E-mail: ishigaki@life.shimane-u.ac.jp*
[b]*Raman Project Center for Medical and Biological Applications, Shimane University, 1060 Nishikawatsu, Matsue, Shimane 690-8504, Japan*
[c]*Bio/Life Science Project, Sales Division, HORIBA, Ltd, 2 Miyanohigashi-cho, Kisshoin, Minami-ku, Kyoto 601-8510, Japan*
[d]*Laboratory of Animal Reproduction, Graduate School of Integrated Science for Life, Hiroshima University, 1-4-4 Kagamiyama, Higashi-Hiroshima, Hiroshima 739-8528, Japan. E-mail: hoshinoy@fc.jwu.ac.jp*

Published on 04 November 2021. Downloaded on 7/17/2025 3:33:19 PM.

ture such as proteins, lipids, and cytochromes in living and fixed mouse oocytes during MI, MII, and germinal vesicle phases using 532 nm Raman imaging.[13] In our previous study, we evaluated oocyte maturity using 785 nm excitation.[14] Well-matured oocytes with high viability competence were identified based on phosphate Raman bands.[14] Furthermore, Ishigaki *et al.* investigated the relationship between embryonic morphological features and biomolecular composition.[15] They proved that embryos with poor morphology had higher lipid concentrations than those with good blastomere features and color.[15]

In this study, Raman spectroscopy was used to assess the degree of oocyte maturation *in situ* at the molecular level. In particular, resonance Raman spectra were obtained from living oocytes using 532 nm excitation, which matches the resonance conditions of reduced cytochromes *b* and *c*. Raman spectra were obtained *in situ* for four different phases of oocyte maturation, and the spectral variations among the phases were investigated. Cytochromes *b* and *c* play important roles in mitochondrial aerobic respiration, and the redox of cytochrome *c* functions to transport electrons within the ATP generating process.[16–18] Generally, oxidative damage to cells begins by the excess generation of reactive oxygen species (ROS), which robs the antioxidant capacity, and the intracellular redox balance tilts to an oxidative state.[19–21] Such an oxidative stress causes mitochondrial dysfunction. The ROS scavenging ability decreases with aging and oocytes are injured by oxidative damage due to ovary aging and post-ovulatory aging.[22,23] Therefore, the mitochondrial function can be evaluated by investigating the redox state of cytochrome *c*. Multivariate analysis such as PCA and multi curve resolution (MCR) of the resonance Raman spectra was used to qualitatively and quantitatively evaluate the change in the relative proportions of the reduced and oxidized cytochrome states. The decrease in respiratory activity was identified by measuring the decrease in the intensity of the resonance Raman signals corresponding to reduced cytochrome *c* over the course of overmaturation. Furthermore, the decrease in lipid metabolism was also determined by detecting the increase in the intensity of Raman signals due to lipids. We defined new indexes to reflect the balance between the decrease in respiratory activity and lipid accumulation, I_{750}/I_{1438} and I_{1127}/I_{1438}, which denote the ratios of the representative Raman peak intensities of reduced cytochrome *c* (750 and 1127 cm^{-1}) to those of lipids (1438 cm^{-1}), and we defined the product of these two ratios as a new parameter to assess the oocyte quality. This parameter successfully classified the oocytes based on their quality, which varied with their degree of maturation. Furthermore, *in vitro* fertilization was performed on oocytes after 15 s of laser irradiation (with a 532 nm excitation and 7.0 mW laser power at the sampling point by continuously scanning the laser spot across a circular area with a 5 μm diameter), and the effect of the laser was evaluated from the developmental rate for the morula and blastocyst stages. The results showed that the Raman measurements were noninvasive.

These results suggest that Raman spectroscopy can be used to noninvasively assess oocyte quality based on the balance between respiration activity and lipid metabolism. Lipids are potent sources of cellular energy, and lipid metabolism is closely related to cell respiration for energy production in the mitochondrial matrix.[24–26] Therefore, an *in situ* assessment of cell activity based on the balance between respiration activity and lipid metabolism has potential application to somatic cells and iPS cells, in addition to oocytes. This study may provide a new general method for evaluating cell activity *in situ*.

Materials and methods

Animals and oocyte collection

ICR mice were purchased from Japan SLC Inc. (Shizuoka, Japan). Immature 20- to 23-day-old female mice were used. An ovulation treatment was performed using 5 IU pregnant mare's serum gonadotropin (PMSG; Teikoku Hormone MFG, Tokyo, Japan), followed by 5 IU human chorionic gonadotropin (hCG; Teikoku Hormone MFG) after 48 h. Oocytes were collected from three female mice at each phase (13, 15, 18 and 24 h after hCG injection), and the four phases were denoted as phases I, II, III and IV. The experimental design followed that of Sakai *et al.*;[27–29] the oocytes had the highest developmental competence in phase II and were overmatured in phase IV. The variation in developmental competence over the course of oocyte maturation is shown in Fig. 1. The oocytes were placed in Leibovitz's L-15 medium (Invitrogen, Grand Island, NY, USA) containing 0.1% polyvinyl alcohol (PVA; Sigma-Aldrich, St Louis, MO, USA). The cumulus cells were removed by treatment with 0.1% hyaluronidase at 37 °C. The reproducibility was confirmed by repeating the experimental procedure three times.

In vitro fertilization and embryo culture

In vitro fertilization and embryo culture were carried out following previously reported methods.[14,30] Spermatozoa were

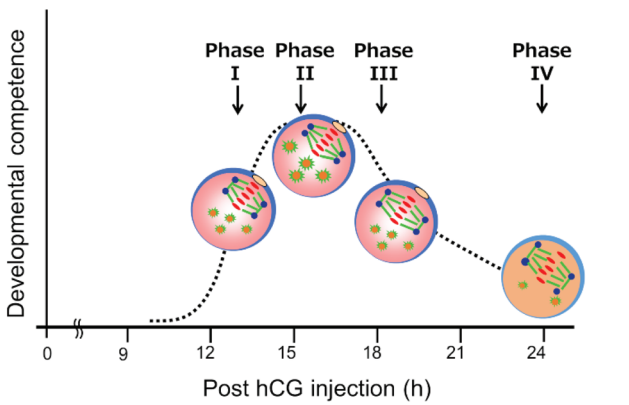

Fig. 1 Variation in developmental competence over the course of oocyte maturation. In oocytes with high developmental competence, the pericentriolar material (PCM) distance between the spindle poles is short and increasing over time. In addition, the expression of the microtubule organizing center in the cytoplasm also becomes strong when PCM is approaching.

This journal is © The Royal Society of Chemistry 2021

Published on 04 November 2021. Downloaded on 7/17/2025 3:33:19 PM.

collected from the cauda epididymis and preincubated for 2 h in 400 μL of HTF medium to enable capacitation before insemination. After capacitation, the spermatozoa were introduced into 200 μL droplets of the fertilization medium at a final concentration of 700 spermatozoa per μL. At 4 h after insemination, the penetration of sperm into the oocytes was confirmed by microscopic examination; the oocytes were subsequently washed thoroughly five times and then cultured in KSOM medium. All the embryos were incubated in 100 μL droplets of the culture medium under a humidified atmosphere of 5% CO_2 in air at 37 °C.

All the experiments were carried out in accordance with the fundamental guidelines for the proper conduct of animal experiments and related activities in academic research institutions under the jurisdiction of the Ministry of Education, Culture, Sports, Science and Technology in Japan. The present study was approved by the Ethics Committee of Hiroshima University and Horiba, Ltd in Japan.

Raman measurement and multivariate analysis

The micro Raman system (LabRAM HR Evolution Raman microscope, Horiba, Kyoto Japan) consisted of a 532 nm DPSS laser, a spectrometer, a 600 gr mm^{-1} holographic grating blazed at 500 nm, an EMCCD scientific camera (SynapseEM, Horiba), and a microscope (an Eclipse Ti2 inverted microscope, Nikon, Tokyo, Japan) with a 60× water emersion objective lens (NA = 1.20, Nikon). The excitation laser power was approximately 7.0 mW at the sampling point, and the exposure time was 15 s (15 s × 1). The system was equipped with a stage-top chamber (BLAST Inc., Kanagawa, Japan), within which the oocytes were maintained in the L-15 medium containing 0.1% PVA at 37 °C during each Raman measurement.

Photothermal damage to the oocytes by laser irradiation was prevented by using a DuoScan™ imaging system (Horiba) to continuously scan the laser spot across a specified circular area (diameter: 5 μm) to obtain an averaged oocyte spectrum. The numbers of oocytes measured at each maturation phase were 44 (I), 58 (II), 59 (III), and 57 (V), and one point at the central part of oocytes was measured for each one, which is relatively uniform with few organelles. The measured Raman spectra were calibrated using the peak for silicon. The wavenumber resolution was 2 cm^{-1}, and the autofluorescence background of the sample was removed using 5^{th}-order polynomial fitting. The spectral intensity was normalized by the standard peak at 1001 cm^{-1} for phenylalanine so that the peak height became 1. The averaged Raman spectra for each developmental stage were calculated from the preprocessed Raman data. PCA was carried out using Unscrambler X 10.3 chemometrics software (Camo Analytics, Oslo, Norway). MCR was performed using an open source of nonnegative matrix factorization, a machine learning library "scikit-learn" (ver. 0.21.1) opened by Python (ver. 3.6.1). After guessing the number of effective components by singular value decomposition (SVD) analysis and confirming that the Raman matrix was decomposed into independent pure components, the MCR calculations were carried out using ingredient and trial numbers of 5 and 1000, respectively. An unpaired two-sided Student's *t*-test was performed on the data set for every two phases to identify significant differences between the pure component concentrations extracted by MCR.

Sample preparation of cytochromes and resonance Raman measurements

Cytochrome *b* (C1427, human, Sigma-Aldrich) and cytochrome *c* (9007-43-6, from an equine heart, Sigma-Aldrich) reagents were diluted with 0.05 M Tris-HCl buffer (pH = 7.6, FUJIFILM Wako Pure Chemical Co., Osaka, Japan) to a final concentration of 4 μM. Cytochrome reduction was carried out by adding sodium dithionite at final concentrations of 2 mM and 50 μM to cytochrome *b* and *c* solutions, respectively. UV-Vis absorbance spectra were obtained before each Raman measurement to determine whether the cytochromes were in oxidized or reduced states. A spectrophotometer (Duetta spectrofluorometer, Horiba) was used to perform the UV-Vis measurements in the 375–650 nm region. The Raman spectra for standard cytochrome solutions were recorded using an XploRA Raman microscope (Horiba) equipped with an extension for macro measurement, a 10× objective lens (NA = 0.25, Olympus, Tokyo, Japan) and a grating (1800 gr mm^{-1}). A 532 nm excitation wavelength was used, the laser power at the sampling point was 11.0 mW, and the exposure time was 120 s (60 s × 2).

Results and discussion

Fig. 2 shows the averaged Raman spectra in the 1800–600 cm^{-1} region obtained for mouse oocytes at phases I (n = 44), II (n = 58), III (n = 59), and IV (n = 57) after the injec-

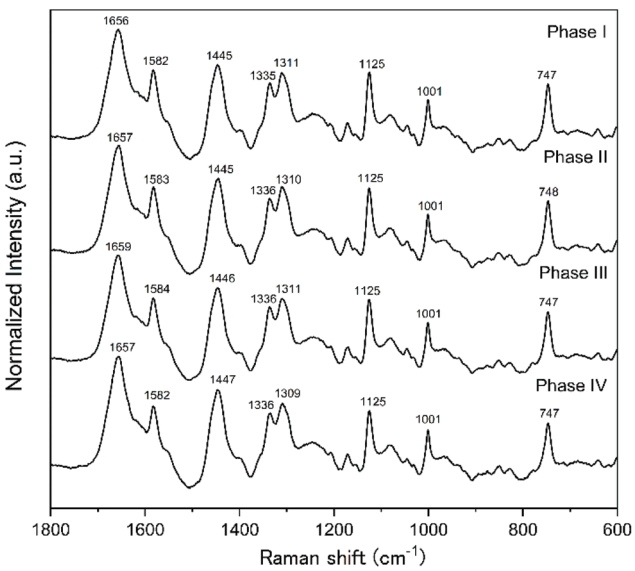

Fig. 2 Averaged Raman spectra in the 1800–600 cm^{-1} region for mouse oocytes obtained at phases I (n = 44), II (n = 58), III (n = 59), and IV (n = 57).

Published on 04 November 2021. Downloaded on 7/17/2025 3:33:19 PM.

tion of hCG hormone. Distinct peaks from proteins, lipids, DNA/RNA, and especially cytochromes can be observed. The peak at 1001 cm^{-1} is associated with phenylalanine ring breathing,[31] and the corresponding peak height was used as an internal standard to normalize the Raman spectra. The band at 1656 cm^{-1} is the overlap of two bands assigned to the amide I modes of proteins and the C=C stretching modes of lipids,[31] and the band at 1445 cm^{-1} arises from the C–H deformation of lipids, proteins, and carbohydrates. The peaks at 1335 and 1311 cm^{-1} are assigned to the CH_3/CH_2 twisting and bending modes.[31] In addition, four prominent peaks associated with reduced cytochromes are observed at 1582, 1311, 1125, and 747 cm^{-1}. The 532 nm excitation wavelength matches the absorption energy of reduced cytochromes *b* and *c*, and the resonance effect remarkably enhanced the intensities of these reduced cytochrome peaks. Table 1 summarizes the peak assignments for the Raman spectra obtained for the oocytes.

The origin of the peaks due to cytochromes, namely, oxidized and reduced cytochromes *b* and *c*, was confirmed. Fig. 3A shows the ultraviolet-visible (UV-Vis) absorbance spectra in the 460–600 nm region for oxidized and reduced cytochromes *b* and *c*. As the reduced cytochromes exhibited absorption maxima near the laser excitation wavelength (532 nm), the resonance resulted in very strong Raman signals from the reduced cytochromes. The enhancement of the Raman signals from the absorption of the oxidized cytochromes deviated from the resonance condition, resulting in less enhanced Raman signals. The Raman spectra of reduced cytochromes *b* and *c* were characterized by typical strong peaks at approximately 1582, 1123, and 750 cm^{-1} (Fig. 3B): the peaks at 1123 and 750 cm^{-1} were assigned to pyrrole half-ring (ν_{22}) and pyrrole ring breathing (ν_{15}) modes, respectively.[31,32] The cytochrome *c* spectrum exhibited a strong peak at 1312 cm^{-1}, whereas the cytochrome *b* spectrum exhibited two peaks at 1338 and 1301 cm^{-1}. A characteristic feature of the cytochrome *c* spectra was the appearance of relatively strong peaks at 690 and 643 cm^{-1}. The abovementioned properties of the resonance Raman spectra of cytochromes *b* and *c* confirmed that the strong peaks (1582, 1311, 1125, and 747 cm^{-1}) in the

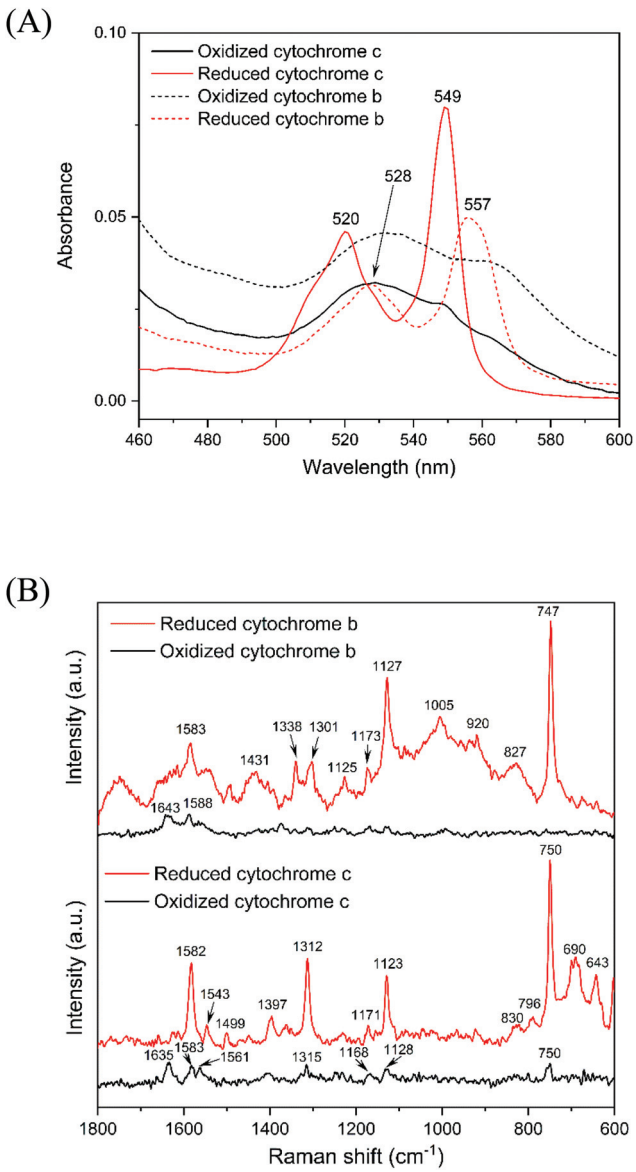

Fig. 3 (A) UV-Vis absorbance spectra (460–600 nm) and (B) 532 nm-excited Raman spectra (1800–600 cm^{-1}) of oxidized and reduced cytochrome *b* and *c*.

Table 1 Peak assignments for Raman spectra obtained for mouse oocytes

Peak (cm^{-1})	DNA/RNA	Proteins	Lipids
742		*Sym* ring br of Try	
747		Cytochromes	
828	*asym* str PO_2^- DNA/RNA	Ring br Tyr	
850		Ring br Tyr	
1001		*Sym* ring br Phe	
1126		C–N str, cytochromes	
1242	T, A	Amide III	=C–H ben
1311–1337		CH_3/CH_2 twi, ben, cytochromes	CH_3/CH_2 twi, ben
1445		CH def	CH def
1582		Cytochromes	
1656		Amide I	C=C str

br: breathing, str: stretching, twi: twisting, ben: bending, def: deformation, *sym*: symmetric, *asym*: asymmetric.

 This journal is © The Royal Society of Chemistry 2021

Published on 04 November 2021. Downloaded on 7/17/2025 3:33:19 PM.

Raman spectra obtained for mouse oocytes at four stages were mainly derived from the reduced cytochromes.

Principal component analysis (PCA)

The spectral variations were analyzed by PCA to determine how the molecular composition changed as the oocytes matured. PCA was performed by selecting the most contralateral group of immature (phase I) and overmature (phase IV) oocytes. Among the combinations of score plots of principal components (PCs) in two dimensions, PC 2 *vs.* PC 3 showed the best pattern of distinguishing between immature and overmature oocytes (Fig. 4A). Fig. 4B shows the loading plots of PC 1 (55.7%), PC 2 (12.6%), and PC 3 (3.2%) for the PCA. The loading plot of PC 1 exhibited strong peaks corresponding to the reduced cytochromes *c*: two peaks at 690 and 641 cm^{-1} and a single peak at 1311 cm^{-1}. In the loading plot of PC 2, three peaks at 1583, 1127, and 750 cm^{-1} and two peaks at 1657 and 1438 cm^{-1} appeared in the negative and positive directions, respectively. The intensities of the three peaks in the negative direction were lower in the overmature phase than in the immature phase. The peak in the positive direction at 1657 cm^{-1} was assigned to the amide I mode of proteins and the C=C stretching modes of lipids, and the peak at 1438 cm^{-1} was assigned to the C–H deformation of proteins, lipids, and hydrocarbons. The intensities of these two peaks increased at the overmature phase.

The averaged spectral intensities at approximately 1657, 1438, 1127, and 750 cm^{-1} for all four phases were compared to confirm the trend in the variation in the spectral intensity identified using PCA. The peak intensities at 1127 and 750 cm^{-1} were the same for phases I and II and then gradually tended to weaken for phases III and IV (Fig. 4C and D) without significant differences about the peak positions between them. All the Raman spectra were normalized to the phenylalanine peak intensity at 1001 cm^{-1}. Therefore, the decrease in the cytochrome *c* peak intensities at 1127 and 750 cm^{-1} for phases

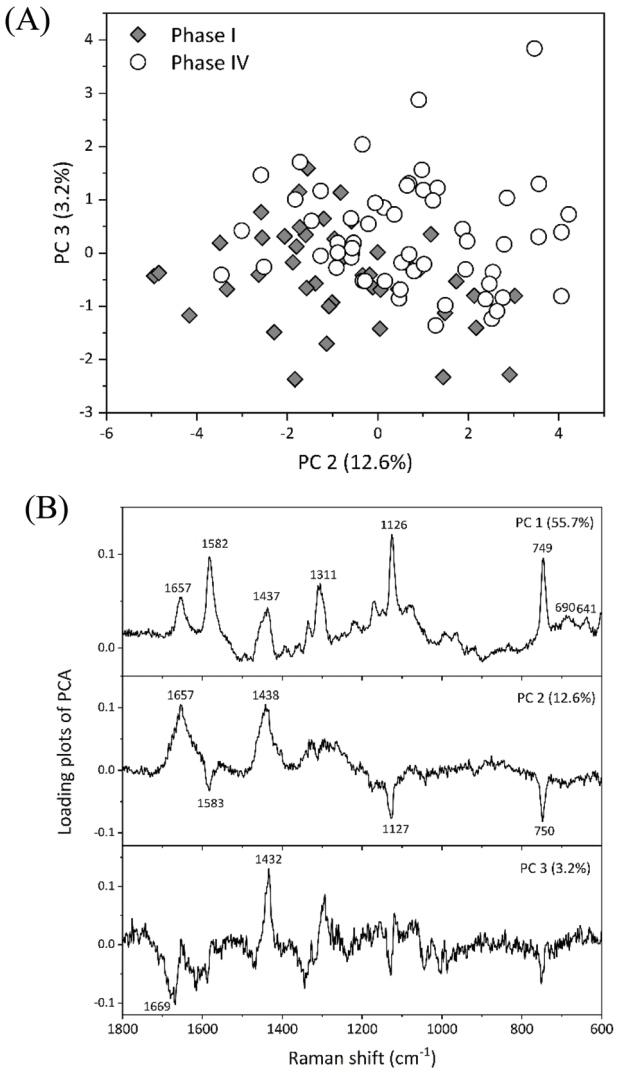

Fig. 4 (A) Score plots of PC2 *vs.* PC3 obtained by PCA; (B) loading plots of PC1, PC2, and PC3 obtained by PCA; and (C) comparison of spectral intensities and (D) the corresponding variations of these intensities at 748, 1127, 1442, and 1652 cm^{-1} for phases I, II, III, and IV. Box plots in (D) are expressed as mean value ± standard deviation (SD), where the central line is mean value, and error bars show the range between minimum and maximum values; significant differences were assessed by the *t*-test (*: $p < 0.05$, **: $p < 0.01$, ***: $p < 0.001$).

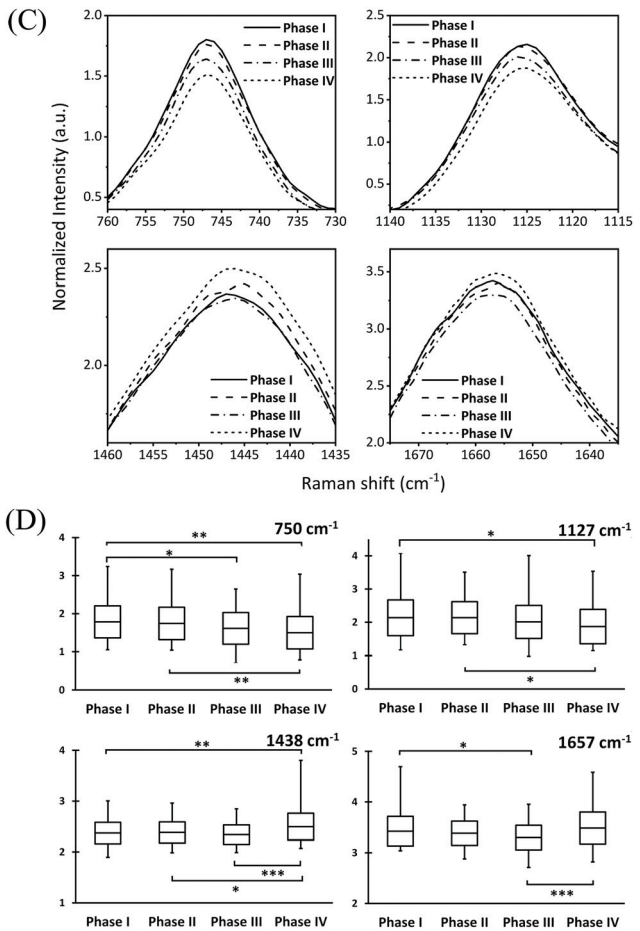

Fig. 4 *(Contd).*

Published on 04 November 2021. Downloaded on 7/17/2025 3:33:19 PM.

III and IV can be interpreted as the deviation of cytochrome *c* from the reduction state, with a corresponding increase in the oxidized cytochrome *c* content. The increase in the peak intensities at 1657 and 1438 cm^{-1} suggested an increase in the relative concentration of molecular compounds other than cytochromes. We previously studied oocyte maturation using 785 nm excitation and found that the concentration of unsaturated fatty acids increased during phase IV.[14] Characteristic fatty acid peaks at 1658 and 1445 cm^{-1} were extracted from the high wavenumber region (1800–1400 cm^{-1}) of the spectrum as an index of overmature oocytes. The two peaks in PC2 appeared at almost the same position (1657 and 1438 cm^{-1}) in this study as in our previous study and are attributed to redundant lipids resulting from abnormal lipid metabolism of overmature oocytes.

Multi curve resolution (MCR) analysis

Molecular composition changes during the maturation of oocytes were semi-quantified using MCR. The spectral data matrix V is a linear combination $V = WH$, where W and H are matrixes of pure component spectra and its intensity profile, respectively.[33] The Raman spectra were decomposed into intrinsic components by MCR with a nonnegative restriction, and the corresponding concentration changes were quantitatively analyzed. Fig. 5A shows the loading plots for the four MCR components. Component 1 (C1) is assigned to a protein based on the following peaks: the sharp peak at 1001 cm^{-1} corresponds to phenylalanine; additional peaks at 742 cm^{-1} arise from tryptophan symmetric breathing modes; tyrosine doublets appear at 850 and 828 cm^{-1}; a C–N stretching peak appears at 1124 cm^{-1}; a broad amide III peak appears at approximately 1242 cm^{-1}; twisting and bending modes of CH_3/CH_2 appear in the 1337–1311 cm^{-1} region; a C–H deformation peak appears at 1446 cm^{-1}; and an amide I peak appears at 1656 cm^{-1}. The detailed Raman peak assignments are summarized in Table 1. The spectral pattern of C1 is very similar to protein-rich spectra obtained from mouse oocytes at 785 nm excitation.[14] Prominent peaks at 1582, 1311, 1126, and 749 cm^{-1} dominated C2, which are used in conjunction with peaks at 690 and 641 cm^{-1} to assign these spectral components to reduced cytochrome *c*. C3 exhibited the spectral pattern of unsaturated fatty acids, which was exactly the same as that obtained for the loading plot of PC1 from the PCA used to identify the overmature oocytes at phase IV in our previous study.[14] C4 also exhibited a cytochrome spectral component. This component was likely to correspond to reduced cytochrome *b*; the spectral features consist of strong peaks at 749, 1128, and 1583 cm^{-1}, a broad peak at approximately 1001 cm^{-1}, and double peaks at 1342 and 1314 cm^{-1}. The higher order components did not show a meaningful spectral pattern due to biological molecules, and the components up to C4 were enough to be discussed as the intrinsic components.

C2 and C3 exhibited interesting variations in concentration with oocyte maturation (Fig. 5B). The reduced cytochrome *c* concentration represented by C2 was high at phases I and II

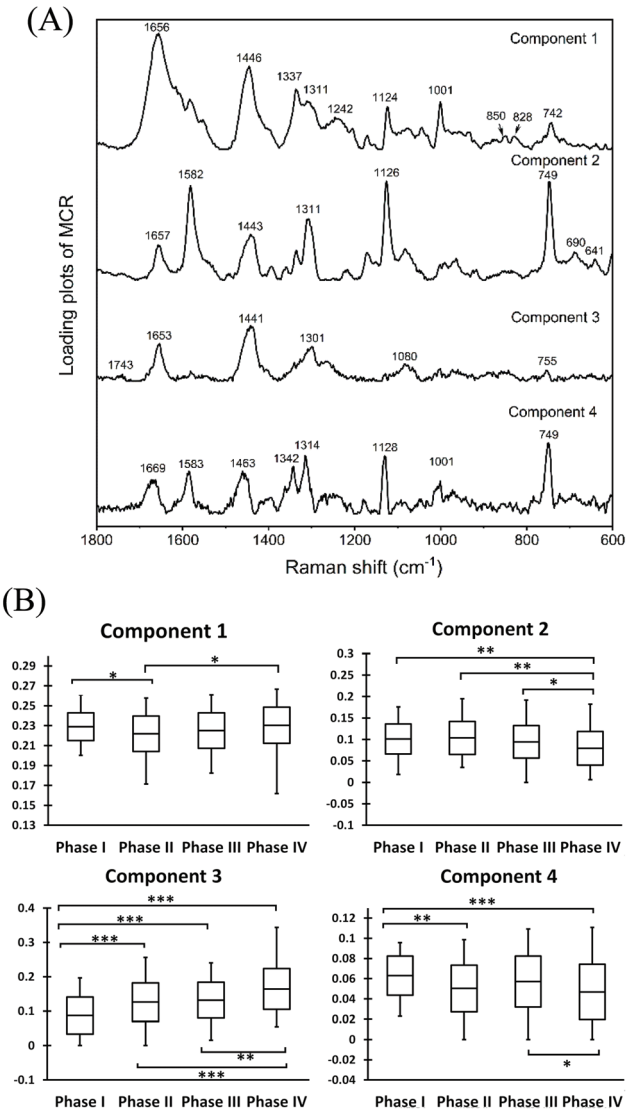

Fig. 5 (A) Spectra of pure components and (B) corresponding variations in concentration extracted by MCR: box plots in (B) are expressed as mean value ± standard deviation (SD), where the central line is the mean value, and error bars show the range between minimum and maximum values; significant differences were assessed by the *t*-test (*: $p < 0.05$, **: $p < 0.01$, ***: $p < 0.001$).

and decreased as the oocytes overmatured during phase IV. The lipid concentration represented by C3 systematically increased with maturation. These results quantitatively show that overmaturation promoted the oxidation of cytochrome *c*, reduced respiratory activity, and decreased metabolism, resulting in lipid accumulation. The MCR results provided a quantitative basis for the concentration variation in *in ovo* components associated with oocyte maturation, which was consistent with the PCA results.

The relationship between respiratory activity and lipid metabolism

Lipid metabolism and cellular respiration are closely related to each other for energy production in the mitochondrial

 This journal is © The Royal Society of Chemistry 2021

Published on 04 November 2021. Downloaded on 7/17/2025 3:33:19 PM.

matrix.[24–26] Fatty acids undergo β-oxidation, the generated acetyl-CoA is incorporated into the citric acid cycle in the mitochondrial matrix, and energy is efficiently produced by aerobic breathing.[34] Carnitine is a vitamin-like substance involved in lipid metabolism that functions in transporting fatty acids into mitochondria. Somfai *et al.* reported that L-cartinine treatment increased the density of activated mitochondria and that the concentration of lipid droplets decreased in porcine oocytes.[35] Dunning *et al.* proved that carnitine treatment promoted β-oxidation to improve oocyte maturation and developmental competence.[19,36] These authors mentioned that the β-oxidation of fatty acids, especially palmitic acid, was also dramatically increased during oocyte maturation. Magnusson *et al.* reported increased oxygen consumption in mature rat oocytes.[37] That is, enhancement of mitochondrial functions due to the activation of lipid metabolism has been shown to result in good maturation. In this study, we successfully detected the activation of respiration and the improvement of lipid metabolism in well-matured oocytes *in situ*, which are the most fundamental biochemical reactions of life.

New discrimination index of oocyte maturation based on balance between respiratory activity and lipid metabolism

A new index for measuring the oocyte quality *in situ* was proposed based on the observed decrease and increase in the relative concentration of reduced cytochrome *c* and lipids, respectively, resulting from the oxidation of cytochrome *c* and reduced lipid metabolism caused by oocyte overmaturation. The proportion of the peak intensities I_{750}/I_{1438} and I_{1127}/I_{1438}, represented by the ratio of Raman peak intensities due to reduced cytochrome *c* (750 and 1127 cm^{-1}) and lipids (1438 cm^{-1}), was defined as the index reflecting the balance between respiratory activity and lipid metabolism; these indexes were comparatively analyzed over the course of maturation. Fig. 6A shows plots of values I_{750}/I_{1438} *vs.* I_{1127}/I_{1438} values. These two ratios tend to be higher for young oocytes, which have a higher concentration of reduced cytochrome *c* and lower lipid accumulation than older oocytes. The data for phase IV were distributed away from the data for the other groups on the plot diagonal.

A threshold for quantitatively assessing oocyte quality was obtained from the frequency distribution of the product of these two indexes ($I_{750}/I_{1438} \times I_{1127}/I_{1438}$) (Fig. 6B). When both indexes are large, the product is also large. If even one of the two indexes is small, the product is small, showing that the oocyte is not in good condition, based on the respiratory activity and lipid metabolism. The product was scarcely higher than one for phase IV but exceeded one for some data in phases I and II (Fig. 6B). Most of the indexes were less than 0.6 for phase IV. The new product index reasonably reproduces the reported trends of oocyte quality. A novel evaluation method of oocyte quality can be constructed by performing *in vitro* fertilization after Raman measurement and defining a threshold area for the index with a high fertilization rate and high viability.

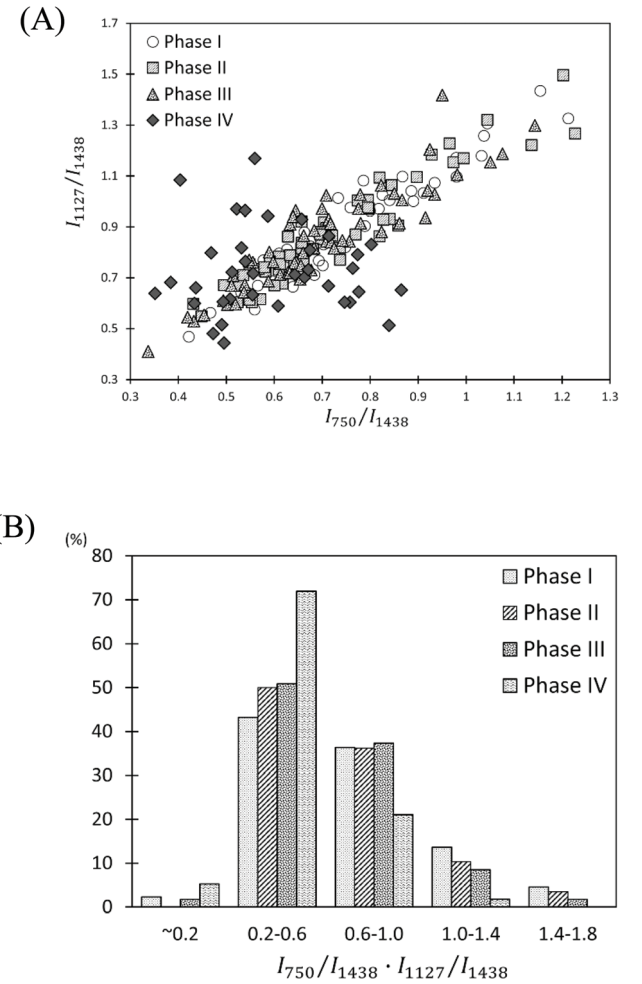

Fig. 6 (A) Score plot of I_{750}/I_{1438} *vs.* I_{1127}/I_{1438} and (B) frequency distribution of the product of I_{750}/I_{1438} and I_{1127}/I_{1438}.

Evaluation of laser invasiveness

In vitro fertilization was carried out for laser-irradiated oocytes, and embryonic development was observed for five days. Fig. 7 shows images of (A) laser-irradiated and (B) nonradiated embryos on the fifth day of incubation. Several blastocysts and morula were observed, some of which were already hatched in both cases.

Fig. 7C shows the developmental rates (%) of oocytes that progressed to morula or blastocyst stages. The total developmental rate to the morula and blastocyst stages in the control was higher than 40% for phases I, II and III. The total developmental rate obtained using the ovulation treatment used in this study has been reported to be 13.4–60.7%.[27] The oocyte maturation rate followed the same trend as has been previously reported, that is, the oocyte maturation rate was highest in phase II and lowest in phase IV. All the developmental results of the control confirmed that oocyte collection was properly carried out.

The laser-irradiated oocytes had a slightly lower developmental rate than the control oocytes for phases I, II and IV. However, the developmental rate of laser-irradiated oocytes was higher than those of the control oocytes for phase III. Thus, the effect of laser irradiation on the development rate

Published on 04 November 2021. Downloaded on 7/17/2025 3:33:19 PM.

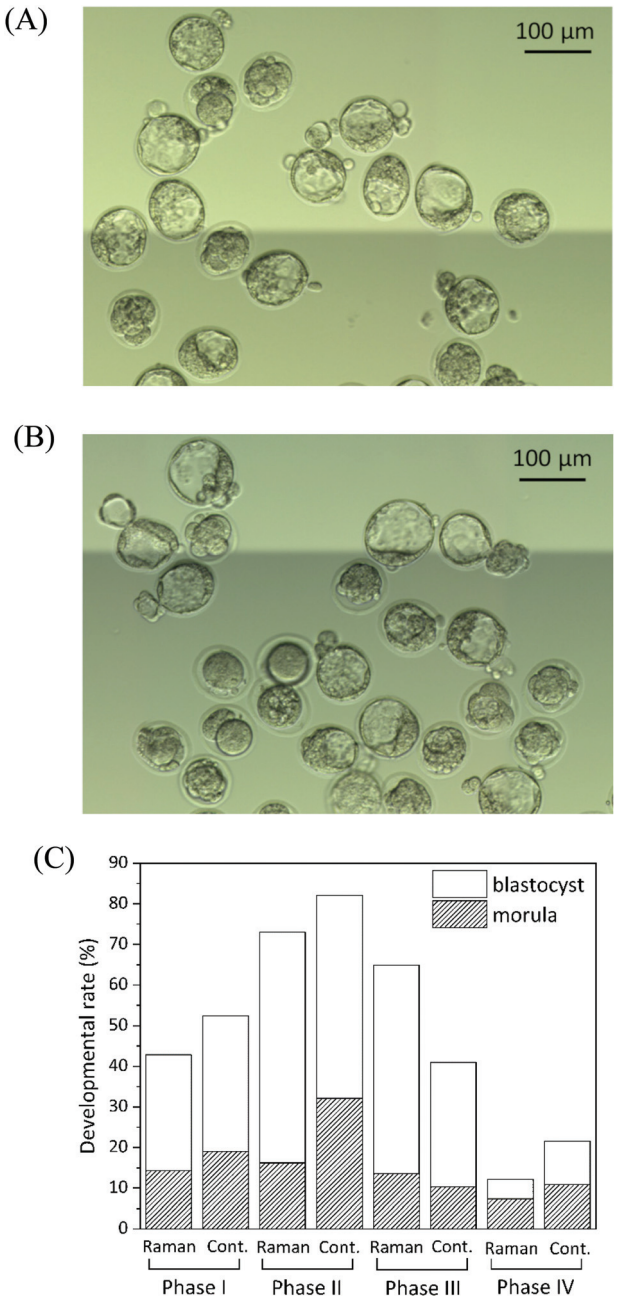

Fig. 7 Image of embryos on 5th day of incubation: (A) laser-irradiated and (B) nonirradiated embryos; (C) developmental rates (%) of oocytes that progressed to morula or blastocyst stages.

could not be confirmed. Therefore, it was concluded that laser irradiation had no effect on the oocytes. Invasiveness of the 532 nm excitation laser on the oocytes was anticipated at the start of the experiments. Consequently, measures were taken to prevent oocyte damage: a low irradiation time and power of 15 s and 7.0 mW, respectively, were used at the sampling points, and the laser irradiation point was moved within a 5 μm circle in a zigzag manner. The results showing the noninvasiveness of the laser irradiation are very useful for practical application of Raman spectroscopy to the assessment of oocyte quality.

Conclusion

In the present study, we used Raman spectroscopy to evaluate the degree of oocyte maturation *in situ* by assessing both respiratory activity and lipid metabolism. The decrease in the intensity of the Raman signal for reduced cytochrome *c* was used to identify the decrease in respiratory activity in overmature oocytes; deviation from the resonance condition was caused by the transition of cytochrome *c* from the reduced state to the oxidized state. Lipid accumulation was found to occur concomitantly with the decrease in respiratory activity. Two new indexes were defined to reflect the balance between decreased respiratory activity and lipid metabolism, *i.e.* two ratios of Raman peak intensities I_{750}/I_{1438} and I_{1127}/I_{1438}, where a value of the product of two indexes above one was used to identify oocytes actively undergoing respiratory and lipid metabolism. Comparing the developmental rate with and without laser irradiation showed that the laser had no significant effect on the rate. These results indicate that Raman spectroscopy can be used to noninvasively evaluate the oocyte quality *in situ* based on respiratory activity and lipid metabolism.

Both the enhancement of mitochondrial functions and the activation of lipid metabolism, which are intrinsically important biochemical reactions of life, were successfully detected in this study. An *in situ* assessment of cell activity based on the balance between respiration activity and lipid metabolism showed that the developed method can be applied to somatic cells and iPS cells, in addition to oocytes. The method may open a new era for cell evaluation *in situ*.

Author contributions

M. I. and Y. H. designed the experiments. Y. H. performed animal surgery and treated the embryo culture. M. I., S. K., and S. W. carried out the Raman measurements and data analysis. M. I. drafted the manuscript, and all the authors approved the manuscript for publication.

Conflicts of interest

There are no conflicts to declare.

Acknowledgements

This work was supported by the JSPS project of the Leading Initiative for Excellent Young Researchers (M. I.), JSPS KAKENHI Grant Number 19K06369 (Y. H.), and Adaptable and Seamless Technology Transfer Program through Target-driven R&D (A-STEP) from JST Grant Number JPMJTR21447297 (M. I. and Y. H.).

This journal is © The Royal Society of Chemistry 2021

Published on 04 November 2021. Downloaded on 7/17/2025 3:33:19 PM.

References

1 I. Hoffmann, P. R. Clarke, M. J. Marcote, E. Karsenti and G. Draetta, *EMBO J.*, 1993, **12**, 53–63.
2 B. Ducommun, P. Brambilla, M. A. Felix, B. R. Franza Jr., E. Karsenti and G. Draetta, *EMBO J.*, 1991, **10**, 3311–3319.
3 M. J. Solomon, T. Lee and M. W. Kirschner, *Mol. Biol. Cell*, 1992, **3**, 13–27.
4 Y. Ozaki, *Appl. Spectrosc. Rev.*, 1988, **24**, 259–312.
5 P. Carey, *Principles of Raman Spectroscopy: Biochemical applications of Raman and resonance Raman spectroscopes* Elsevier, Amsterdam, 2012.
6 L. P. Choo-Smith, H. G. M. Edwards, H. P. Endtz, J. M. Kros, F. Heule, H. Barr, J. S. Robinson Jr., H. A. Bruining and G. J. Puppels, *Biopolymers*, 2002, **67**, 1–9.
7 J. W. Chan, D. S. Taylor, T. Zwerdling, S. M. Lane, K. Ihara and T. Huser, *Biophys. J.*, 2006, **90**, 648–656.
8 Y. Tan, S. O. Konorov, H. G. Schulze, J. M. Piret, M. W. Blades and R. F. Turner, *Analyst*, 2012, **137**, 4509–4515.
9 M. Okada, N. I. Smith, A. F. Palonpon, H. Endo, S. Kawata, M. Sodeoka and K. Fujita, *Proc. Natl. Acad. Sci. U. S. A.*, 2012, **109**, 28–32.
10 M. Kakita, V. Kaliaperumal and H. O. Hamaguchi, *J. Biophotonics*, 2012, **5**, 20–24.
11 B. Davidson, A. A. Murray, A. Elfick and N. Spears, *PLoS One*, 2013, **8**, e67972.
12 L. Bogliolo, O. Murrone, G. Di Emidio, M. Piccinini, F. Ariu, S. Ledda and C. Tatone, *J. Assist. Reprod. Genet.*, 2013, **30**, 877–882.
13 P. Heraud, K. M. Marzec, Q. H. Zhang, W. S. Yuen, J. Carroll and B. R. Wood, *Sci. Rep.*, 2017, **7**, 8945.
14 M. Ishigaki, Y. Hoshino and Y. Ozaki, *Analyst*, 2019, **144**, 1527–1534.
15 M. Ishigaki, K. Hashimoto, H. Sato and Y. Ozaki, *Sci. Rep.*, 2017, **7**, 43942.
16 T. Takano and R. E. Dickerson, *Proc. Natl. Acad. Sci. U. S. A.*, 1980, **77**, 6371–6375.
17 S. Ferguson-Miller, D. L. Brautigan and E. Margoliash, *J. Biol. Chem.*, 1976, **251**, 1104–1115.
18 M. Degli Esposti, S. De Vries, M. Crimi, A. Ghelli, T. Patarnello and A. Meyer, *Biochim. Biophys. Acta, Bioenerg.*, 1993, **1143**, 243–271.
19 A. Y. Andreyev, Y. E. Kushnareva and A. A. Starkov, *Biochemistry*, 2005, **70**, 200–214.
20 A. Trifunovic and N. G. Larsson, *J. Intern. Med.*, 2008, **263**, 167–178.
21 G. Lenaz, C. Bovina, M. D'aurelio, R. Fato, G. Formiggini, M. L. Genova, G. Giuliano, M. M. Pich, U. Paolucci, G. P. Castelli and B. Ventura, *Ann. N. Y. Acad. Sci.*, 2002, **959**, 199–213.
22 C. Tatone, M. C. Carbone, S. Falone, P. Aimola, A. Giardinelli, D. Caserta, R. Marci, A. Pandolfi, A. M. Ragnelli and F. Amicarelli, *Mol. Hum. Reprod.*, 2006, **12**, 655–660.
23 A. P. Goud, P. T. Goud, M. P. Diamond, B. Gonik and H. M. Abu-Soud, *Free Radicals Biol. Med.*, 2008, **44**, 1295–1304.
24 K. R. Dunning, K. Cashman, D. L. Russell, J. G. Thompson, R. J. Norman and R. L. Robker, *Biol. Reprod.*, 2010, **83**, 909–918.
25 T. Watanabe, A. Thayil, A. Jesacher, K. Grieve, D. Debarre, T. Wilson, M. Booth and S. Srinivas, *BMC Cell Biol.*, 2010, **11**, 38.
26 P. Haggarty, M. Wood, E. Ferguson, G. Hoad, A. Srikantharajah, E. Milne, M. Hamilton and S. Bhattacharya, *Hum. Reprod.*, 2006, **21**, 766–773.
27 C. Sakai, Y. Hoshino, Y. Sato and E. Sato, *J. Assist. Reprod. Genet.*, 2011, **28**, 157–166.
28 Y. Sugano, M. Yazawa, S. Takino and S. Niimura, *Zygote*, 2016, **24**, 900–908.
29 A. H. Gates, C. H. Donaldson and M. D. Levy, *Teratology*, 1981, **24**, 321–327.
30 Y. Hoshino and E. Sato, *Dev. Biol.*, 2008, **314**, 215–223.
31 Z. Movasaghi, S. Rehman and I. U. Rehman, *Appl. Spectrosc. Rev.*, 2007, **42**, 493–541.
32 J. L. Deng, Q. Wei, M. H. Zhang, Y. Z. Wang and Y. Q. Li, *J. Raman Spectrosc.*, 2005, **36**, 257–261.
33 D. D. Lee and H. S. Seung, *Nature*, 1999, **401**, 788–791.
34 J. R. Williamson and R. H. Cooper, *FEBS Lett.*, 1980, **117**, 73–85.
35 T. Somfai, M. Kaneda, S. Akagi, S. Watanabe, S. Haraguchi, E. Mizutani, T. Q. Dang-Nguyen, M. Geshi, K. Kikuchi and T. Nagai, *Reprod., Fertil. Dev.*, 2011, **23**, 912–920.
36 K. R. Dunning, D. L. Russell and R. L. Robker, *Reproduction*, 2014, **148**, 15–27.
37 C. Magnusson, T. Hillensjö, A. Tsafriri, R. Hultborn and K. Ahrén, *Biol. Reprod.*, 1977, **17**, 9–15.